

A magnetoelectric receiving antenna with a bridge-supporting structure for ultralow-frequency wireless communication

Boyu Xin(辛柏雨), Qianshi Zhang(张千十), Lizhi Hu(胡立志), Zishuo Fan(范梓烁), Jie Jiao(焦杰), Chun-Gang Duan(段纯刚), and Anran Gao(高安然)

Citation: Chin. Phys. B, 2025, 34 (**12**): 128401. DOI: 10.1088/1674-1056/adea57
http://cpb.iphy.ac.cn; http://iopscience.iop.org/cpb

What follows is a list of articles you may be interested in

A low-cost invasive microwave ablation antenna with a directional heating pattern

Zhang Wen(文章), Xian-Qi Lin(林先其), Chen-Nan Li(李晨楠), and Yu-Lu Fan(樊钰璐)
Chin. Phys. B, 2022, 31 (**3**): 038401. DOI: 10.1088/1674-1056/ac1e1b

Design and optimization of nano-antenna for thermal ablation of liver cancer cells

Mohammad Javad Rabienejhad, Azardokht Mazaheri, and Mahdi Davoudi-Darareh
Chin. Phys. B, 2021, 30 (**4**): 048401. DOI: 10.1088/1674-1056/abd38e

Stretchable electromagnetic interference shielding and antenna for wireless strain sensing by anisotropic micron-steel-wire based conductive elastomers

Xiaoyu Hu(胡晓宇), Linlin Mou(牟琳琳), and Zunfeng Liu(刘遵峰)
Chin. Phys. B, 2021, 30 (**1**): 018401. DOI: 10.1088/1674-1056/abc2b3

Dual-polarized lens antenna based on multimode metasurfaces

Hao-Fang Wang(王浩放), Zheng-Bin Wang(王正斌), Yong Cheng(程勇), Ye-Rong Zhang(张业荣)
Chin. Phys. B, 2018, 27 (**11**): 118401. DOI: 10.1088/1674-1056/27/11/118401

Correction of failure in antenna array using matrix pencil technique

S U Khan, M K A Rahim
Chin. Phys. B, 2017, 26 (**6**): 068401. DOI: 10.1088/1674-1056/26/6/068401

A magnetoelectric receiving antenna with a bridge-supporting structure for ultralow-frequency wireless communication

Boyu Xin(辛柏雨)[1], Qianshi Zhang(张千十)[1], Lizhi Hu(胡立志)[2], Zishuo Fan(范梓烁)[1], Jie Jiao(焦杰)[3], Chun-Gang Duan(段纯刚)[1], and Anran Gao(高安然)[1,†]

[1] *Key Laboratory of Polar Materials and Devices (MOE), East China Normal University, Shanghai* 200241, *China*
[2] *School of Materials Science and Engineering, Nanjing University of Science and Technology, Nanjing* 210094, *China*
[3] *State Key Laboratory of Functional Crystals and Devices, Shanghai Institute of Ceramics, Chinese Academy of Sciences, Shanghai* 201899, *China*

(Received 9 April 2025; revised manuscript received 29 May 2025; accepted manuscript online 1 July 2025)

The ultralow-frequency (ULF) miniaturized communication device is a development trend and has prospects in underwater environments. In this work, a magnetoelectric (ME) laminate was prepared by magnetostrictive Metglas and piezoelectric PMN-PT, and the electromechanical resonance (EMR) frequencies of the ME laminate were lowered through the bridge-supporting structure. Experiments showed that the supporting structure excited EMR frequencies of 646 Hz, 1089 Hz and 1506 Hz; the ME coefficients were 44.2 nC/Oe, 104.1 nC/Oe and 39.8 nC/Oe, respectively. Next, the ME laminate was assembled to a receiving antenna to receive binary frequency shift keying (2FSK) and binary amplitude shift keying (2ASK) signals accurately.

Keywords: magnetoelectric laminate, receiving antenna, ultralow frequency wireless communication

PACS: 84.40.Ba, 75.80.+q, 07.55.Ge

DOI: 10.1088/1674-1056/adea57 **CSTR:** 32038.14.CPB.adea57

1. Introduction

With the continuous innovation of information technology, the development of underwater communication equipment tends to be miniaturized, has high precision and low power consumption.[1,2] When the electromagnetic waves propagate in the lossy medium, the field intensity decreases exponentially,[3] which means electromagnetic waves decay faster in water than in air, and electromagnetic waves with higher frequencies attenuate faster. Ultralow-frequency (ULF) (300 Hz–3 kHz) electromagnetic waves attenuate slowly, and are more suitable for underwater communication. The reliability and accuracy of underwater information transmission can be enhanced by enhancing the radiation capability of the transmitting antenna or lowering the signal receiving limit of the receiving antenna. Compared with traditional small electric antennas and some conventional low-frequency antennas, magnetoelectric (ME) antennas exhibit strong competitiveness in size and receiving efficiency due to their efficient electromagnetic–mechanical coupling ability,[4] which is a competitive solution for underwater receiving antenna.

The ME effect refers to polarization changes with an external magnetic field, or the magnetization changes with an external electric field, making the ME material a promising material.[5–9] Recently, ME laminate combining acoustic resonance and magnetoelectric effects (ME effects) has attracted extensive attention and has been proved to be a new way to break the limitations of traditional radiation theory.[10,11] Compared with traditional antennas, ME laminates have the advantages of high sensitivity, low cost, miniaturization and low power consumption; they provide great possibility for miniaturization in wireless communication systems, such as wearable monitoring systems and biological communication technologies.[1,2,12–14] They are also a feasible solution for underwater communication.[15–17]

The structure of the ME antenna was first proposed by Yao in 2015, and they analyzed the multiferroic laminate using a one-dimensional finite-difference time-domain method, demonstrating the feasibility of ME laminate from the quality factor.[18] When ME laminates are used in receiving antenna, they often work at their electromechanical resonance (EMR) frequency to obtain the lowest noise equivalent magnetic field and the highest responsivity and receiving capability. However, due to the characteristics of the ME laminate, its resonant frequency is usually tens of kHz, which is difficult to apply to underwater wireless communication. To lower the operating frequency of ME laminates, the material's vibration mode, material size gradient, DC bias magnetic field and load change are usually used as adjustable parameters.[19–24]

In 2017, Sun *et al.* first verified the feasibility of an ME antenna via experiments, its EMR frequency was in the very high frequency (VHF, 30 MHz–300 MHz) band.[25] Subsequently, Sun *et al.* designed an ME transceiver system working in the very low frequency (VLF, 3 kHz–30 kHz) band.[26] Viehland *et al.* prepared an ME laminate based

†Corresponding author. E-mail: argao@clpm.ecnu.edu.cn

© 2025 Chinese Physical Society and IOP Publishing Ltd. All rights, including for text and data mining, AI training, and similar technologies, are reserved.

on magnetostrictive phase (Metglas 2605 amorphous ribbons) and PZT (lead zirconate titanate piezoelectric ceramics, $Pb(Zr_{1-x}Ti_x)O_3$) in 2019; its resonant frequency is about 28 kHz.[27] Wang *et al*. proposed an asymmetric structure to excite the bending vibration mode, which can reduce the resonant frequency from VLF to ULF or even superlow frequency (SLF).[28] They obtained an EMR frequency of 210 Hz, and the noise equivalent magnetic field reached 0.3 pT/rtHz.

Here, we propose a ULF ME receiving antenna with a bridge-supporting structure. We used the bridge-supporting structure to amplify the effects of bending resonance mode; three EMR frequencies in the ULF band were excited. The proposed ME laminate was packaged into an ME receiving antenna with a low-noise charge amplifier. The proposed antenna has a low noise level and strong signal reception capability, can receive the binary frequency shift keying (2FSK) and the binary amplitude shift keying (2ASK) modulation signals effectively, and is expected to be used in underwater wireless communication.

2. Design and principle of ME laminate

As shown in Fig. 1(a), the proposed ME laminate consists of magnetostrictive Metglas 2605 amorphous ribbons (140 mm×20 mm×0.025 mm) and piezoelectric single crystal $0.7Pb(Mg_{1/3}Nb_{2/3})O_3$–$0.3PbTiO_3$ (PMN-PT) plates (40 mm×2 mm×0.5 mm). The magnetostrictive phase is composed of 6 layers of Metglas bonded by epoxy resin, and the piezoelectric phase is composed of 7 piezoelectric single crystal PMN-PT connected through a flexible circuit board. As shown in Fig. 1(b), the piezoelectric phase polarizes along the thickness direction, and the magnetostrictive phase magnetizes along the length direction, which is the "L-T" mode. The two phases were combined with epoxy resin to form an asymmetric structure. This mode requires minimal H_{DC} bias, which is beneficial for enhancing system integration and portability.[29,30]

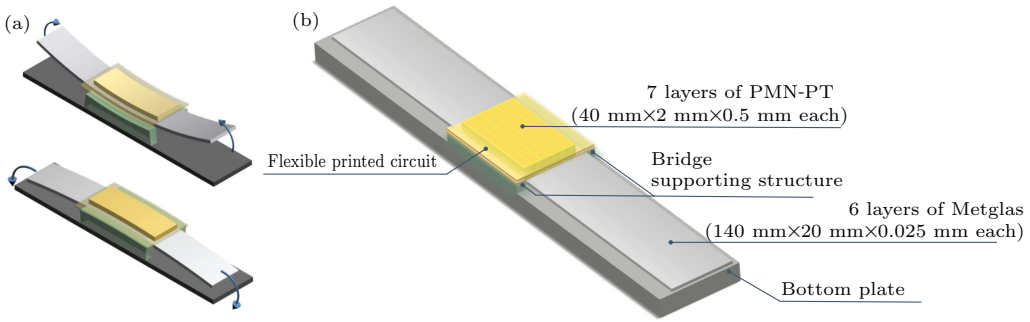


Fig. 1. (a) The principle of the proposed ME laminate. (b) Schematics of the ME laminate.

In this work, the proposed ME laminate antenna features an innovative bridge-supporting structure. This supporting structure enhances the bending vibration mode, effectively lowering the antenna's operating frequency. Specifically, the bridge-supporting structure increases the deformation space of the material, enabling the antenna to operate stably within the ULF range and significantly improving its signal reception capability. The design of the supporting structure optimizes the antenna's performance, allowing it to exhibit excellent reception capability in low-frequency communication.

Based on the "magneto-elastic-electric" coupling between two phases, ME laminate converts magnetic signals to electrical signals:

$$\frac{\mathrm{d}E}{\mathrm{d}H} = k_1 k_2 \cdot n(1-n) \cdot \frac{\mathrm{d}S}{\mathrm{d}H} \times \frac{\mathrm{d}E}{\mathrm{d}S}. \tag{1}$$

Due to the external magnetic field, the piezomagnetic phase generates strain. This mechanical strain will be transferred to the piezoelectric phase through the coupling layer between the two phases, and the piezoelectric phase generates electric polarization due to the piezoelectric effect. Here, $\mathrm{d}E/\mathrm{d}H$ indicates the ME coefficient of the ME laminate; $\mathrm{d}S/\mathrm{d}H$ and $\mathrm{d}E/\mathrm{d}S$ represent the magnetostrictive effect and piezoelectric effect, respectively; n and $1-n$ represent the volume fraction of the two phases; and k_1 and k_2 represent the proportional coefficients of the weakening caused by the two phases interacting with each other.

There are two main resonance modes of ME laminate: length and bending. In the common sandwich structure (magnetostrictive-piezoelectric-magnetostrictive) and most symmetric structures, there is generally only one main EMR peak caused by the length mode, and this is mostly located in the VLF band or low-frequency (LF, 30 kHz–300 kHz) band.[26,31,32] In addition, some asymmetric structures will resonate in bending mode. Previous studies have shown that bending mode will cause a lower EMR frequency.[28,33] The appearance of bending mode is due to the different forces and stress constraints of each part, which leads to the difference in shape variables of each part.

In this work, it is mainly reflected in the difference in the deformation quantities between the upper and lower surfaces of the two phases: when the magnetostrictive phase is

extended because of an external magnetic field, the deformation of the upper surface is smaller than the lower surface due to the restriction of the piezoelectric phase; the lower surface of the piezoelectric phase is elongated by the magnetostrictive phase, and the deformation is larger than the upper surface. In brief, ME laminate has the tendency to bend upwards. Conversely, when the magnetostrictive phase is shortened, the ME laminate has the tendency to bend downward, as shown in Fig. 1(a). It can be seen that in a certain range, the larger the deformation space, the more deformation quantity the ME laminate will have.

The bridge-supporting structure effectively excites multiple bending resonance peaks by altering the boundary conditions. Traditional flat-placed structures typically have "fixed at both ends" boundary conditions, which introduce significant damping and suppress the excitation of higher-order bending modes. In contrast, the bridge structure significantly increases the system's degrees of freedom. The reduction in effective stiffness allows for the excitation of more high-order bending modes.[34]

Additionally, the asymmetric laminate design of the ME laminate causes a shift in the neutral axis, creating strain distribution differences across different regions, which further excites multi-order modes.[35] In terms of energy transfer, the bridge structure reduces substrate contact friction damping, allowing more energy to be retained within the material, thus enhancing the strain coupling efficiency and facilitating the excitation of more high-order resonance modes. Overall, the bridge-supporting structure, through its asymmetric laminate design, suspended boundary conditions, and material stiffness gradient, breaks the symmetry constraints of traditional structures, enabling the coexistence of multi-order bending modes, and providing a theoretical foundation for the design of multi-band ULF ME antennas.

We glued a flexible printed circuit (FPC) with a pair of supporting plates, forming the bridge structure, making the ME laminate completely suspended (hereinafter referred to as the "bridge ME laminate/antenna"). Compared to classical structures, where the ME laminate is placed on a flat surface (hereinafter referred to as the "classic ME laminate/antenna"), the bridge structures can increase the deformation space to amplify the effects of bending resonance mode. Experiments show that the bridge ME laminate has three resonant peaks in the ULF band. Moreover, the resonant peak caused by length resonance mode still exists.

3. Test results and analysis

Figure 2 shows the performance characterization of two kinds of ME laminate. The ME coefficient was tested according to the configuration in Fig. 2(a). Figure 2(b) shows the ME coefficient of classic ME laminate. The EMR frequency ($\sim$ 15 kHz) was caused by length resonance mode. Figure 2(c) shows the ME coefficient of the bridge ME laminate. The EMR frequency of 14.8 kHz was caused by the first-order length resonance mode; it still exists after using the bridge.

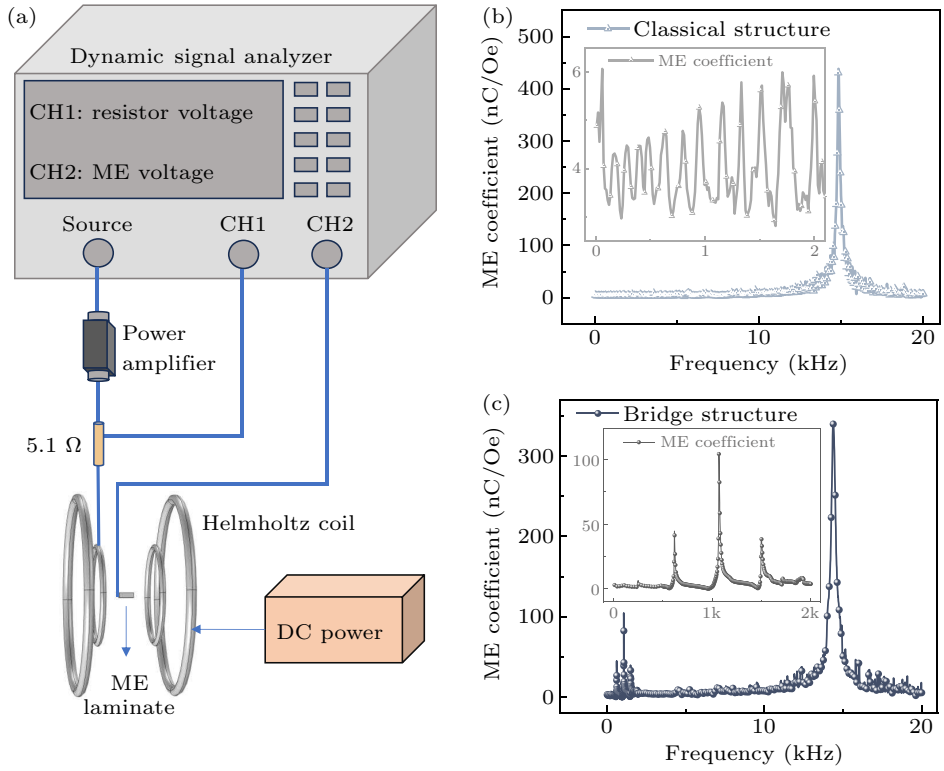


Fig. 2. (a) The configuration for measuring the ME coefficient. The ME coefficients of the classic laminate (b) and bridge ME laminate (c).

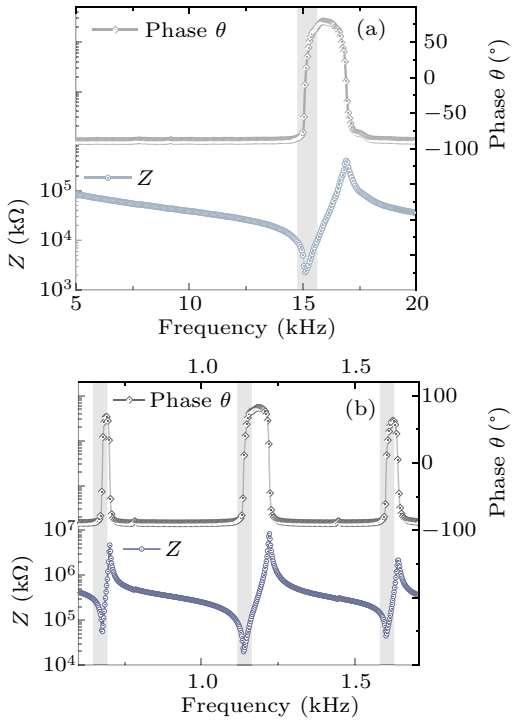


Fig. 3. The impedance spectra of the classic ME laminate (a) and bridge ME laminate (b).

Moreover, the bridge structure enlarged the deformation space and amplified the effects of bending mode sharply. The three EMR peaks ($\sim$ 1 kHz) were exited and can be clearly observed: 646 Hz (f_1), 1089 Hz (f_2) and 1506 Hz (f_3). The resonant ME coefficients shown in Fig. 2(c) are 10–20 times higher than the quasi-static ME coefficients shown in Fig. 2(b). The ME coefficients of the three EMR peaks are 44.2 nC/Oe, 104.1 nC/Oe and 39.8 nC/Oe. The bridge ME laminate was used in the following experiments. The impedance and phase degree of the classic and bridge structures were measured using an impedance analyzer in Figs. 3(a) and 3(b). The impedance further proves the appearance of three resonant peaks after using the support structure.

A DC bias magnetic field has a significant effect on the ability to convert magnetism and electricity. We tested the change in the ME coefficient and EMR frequency with the change in the DC bias (0–10 Oe) magnetic field; the ME coefficients of three frequencies are optimal at 7 Oe, as shown in Fig. 4(b). In addition, a slight dispersion of the resonance frequencies was observed with varying DC bias, which can be attributed to the intrinsic frequency-dependent characteristics of ME laminates.[36] After adjustment and testing, the magnets were fixed in the corresponding position. Next, the ME laminate was packaged in a 3D-printed enclosure with an amplifying circuit and a pair of ferrites, as shown in Fig. 4(a). The charge amplifier amplifies the electrical signal generated by the ME laminate, facilitating the observation and processing of signals. Figure 4(c) shows the response linearity of the ME antenna at three resonant frequencies in the magnetic field intensity range of 2 fT–10 nT. It can be seen that the ME antenna shows high linearity in a wide range, and demonstrates great reliability.

The noise equivalent magnetic field (NEB) is given by

$$\mathrm{NEB} = \frac{\text{ME coefficient (V/T)}}{\text{Noise (V}/\sqrt{\text{Hz}})}. \tag{2}$$

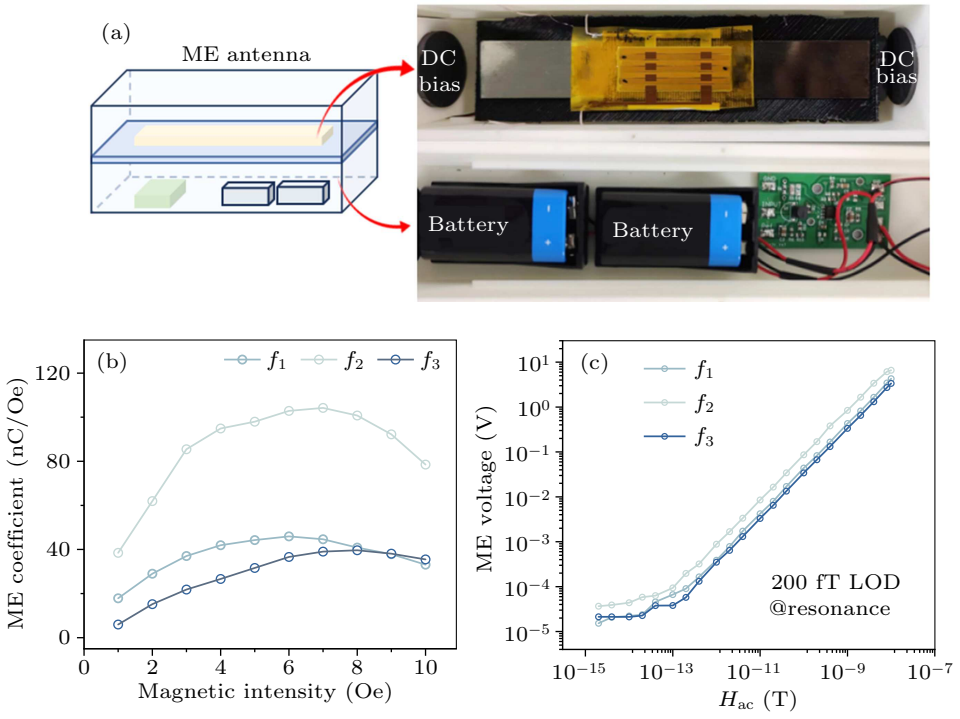


Fig. 4. (a) A schematic of the ME antenna. (b) The ME coefficients change with the DC bias magnetic field. (c) The linearity fitting curve of the ME antenna at three ULF frequencies.

The NEB represents the detection limit of the weak magnetic signal of the ME receiving antenna. The intrinsic noise and the NEB at EMR frequencies are shown in Figs. 5(a) and 5(b). The magnetic field detection limits of the ME antenna at 646 Hz, 1089 Hz and 1506 Hz are 65.33 fT/$\sqrt{\text{Hz}}$,70.92 fT/$\sqrt{\text{Hz}}$ and 126.04 fT/$\sqrt{\text{Hz}}$, respectively. The minimum noise equivalent magnetic field is 65.33 fT/$\sqrt{\text{Hz}}$. The PMN-PT single crystal has low noise and high ME responsivity, and the charge amplifier has low noise and high magnification. Consequently, the noise level was reduced and the ability of the ME antenna to receive electromagnetic wave signals was improved greatly.

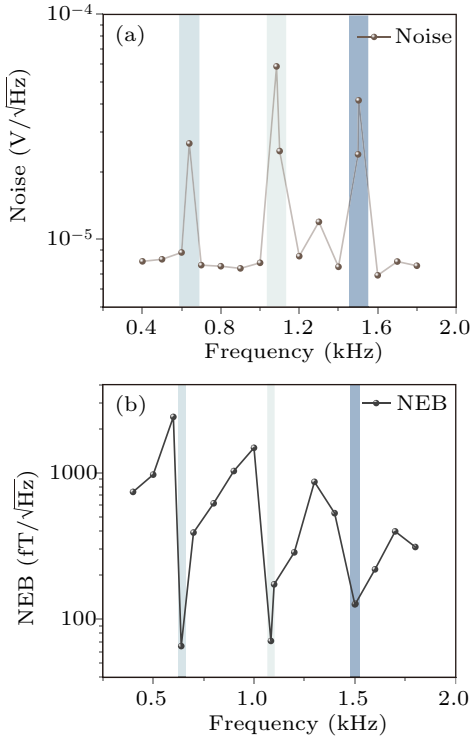


Fig. 5. (a) The noise diagram and (b) the noise equivalent magnetic field of the ME antenna.

4. ULF communication

In the process of transmission, the signal will be converted many times, the original signal needs to be converted by the transmitter into a form that is suitable for signal transmission (modulation). It is crucial that the signal modulation method is suitable for the ME receiving antenna in the signal transmission. According to the different types of signals, modulation methods are divided into analog modulation and digital modulation. Digital modulation has better anti-interference ability, and the signal attenuation is slower. When there are electrical appliances or signal sources working nearby, this method can minimize their interference.[37,38] 2ASK and 2FSK are common digital modulation methods; the amplitude or frequency of the modulated signal are regulated by changing input data bits.

The binary "0" and "1" in the bitstream of 2ASK correspond to two amplitude-varying states of the carrier, which represent off or on in mechanical systems; the switching speed can be controlled by the input bitstream. We used noncoherent demodulation (envelope detection) of 2ASK and tested the signal receiving capability of the ME antenna. Figure 6(a) shows the experimental setup. The ULF electromagnetic wave was emitted by a Helmholtz coil, and the ME antenna received the electromagnetic wave of three EMR frequencies, respectively. As shown in Fig. 6(b)(i), the 1 V_p driven voltage was applied to the Helmholtz coil through a 2× power amplifier. The 1 Hz binary bitstream (0101010101) was used to modulate the original 1089 Hz (f_2) electric signal. Figure 6(b)(ii) is the original modulating signal transmitted by the Helmholtz coil. Figure 6(b)(iii) shows the signal received by the ME antenna. After the filter and the multiplicator, the envelope of f_2 is shown in Fig. 6(b)(iv). The signals were demodulated through a low-pass filter. The original bit stream was successfully restored in Fig. 6(b)(v).

For 2FSK, the binary "0" and "1" in the bitstream correspond to the two frequencies of the carrier signals. The 2FSK can realize continuous or discontinuous phase modulation.[39,40] Compared with 2ASK, it is much less limited by the amplitude of the carrier signal, and can transmit more complex and richer audio and image information.

We tested the 2FSK signal receiving capability of the bridge ME antenna. Because of the similar responsivity, f_1 and f_3 (646 Hz and 1506 Hz) were used to detect 2FSK signals. The 1 Hz bitstream (0101010101) was input to modulate the carrier, as shown in Fig. 6(c)(i). The data acquisition card was controlled by the upper computer to generate 2FSK signals with an amplitude of 1 V_p (646 Hz and 1506 Hz), which were applied to the Helmholtz coil through a 2× power amplifier. Figure 6(c)(ii) is the original modulating signal. The ME receiving antenna was placed 3 m away from the Helmholtz coil; the original time-domain signals received are shown in Fig. 6(c)(iii). After the noncoherent modulation, the envelopes of f_1 and f_3 are shown in Fig. 6(c)(iv). By sampling and judging the amplitudes of f_1 and f_3, the demodulation signals are shown in Fig. 6(c)(v): the original bitstream was precisely recovered.

Figures 6(d) and 6(e) show the 2ASK and 2FSK signal modulation and transmission of the classic ME antenna. Similarly, we applied the same driven voltage to the Helmholtz coil, there are no resonant peaks in the ULF band and the response of FSK is 8 times lower than the bridge antenna. The accurate signal reception and compatibility with multiple modulation methods of the ME antenna demonstrate its strong potential in ULF communication systems.

The proposed ME antenna is compared with several reported alternatives in Table 1, where it demonstrates signif-

icant advantages in low-frequency reception and modulation versatility. Its bridge-supporting structure enhances the bending vibration mode, enabling operation at lower frequencies and more efficient signal reception. This improved performance underscores its strong potential for ULF communication applications.

Additionally, despite a slight difference in voltage coefficient compared to other antennas, the design and optimization undertaken have resulted in a significant improvement in both signal stability and reception sensitivity. These comparison results further demonstrate the proposed ME antenna's application potential in low-frequency communication systems.

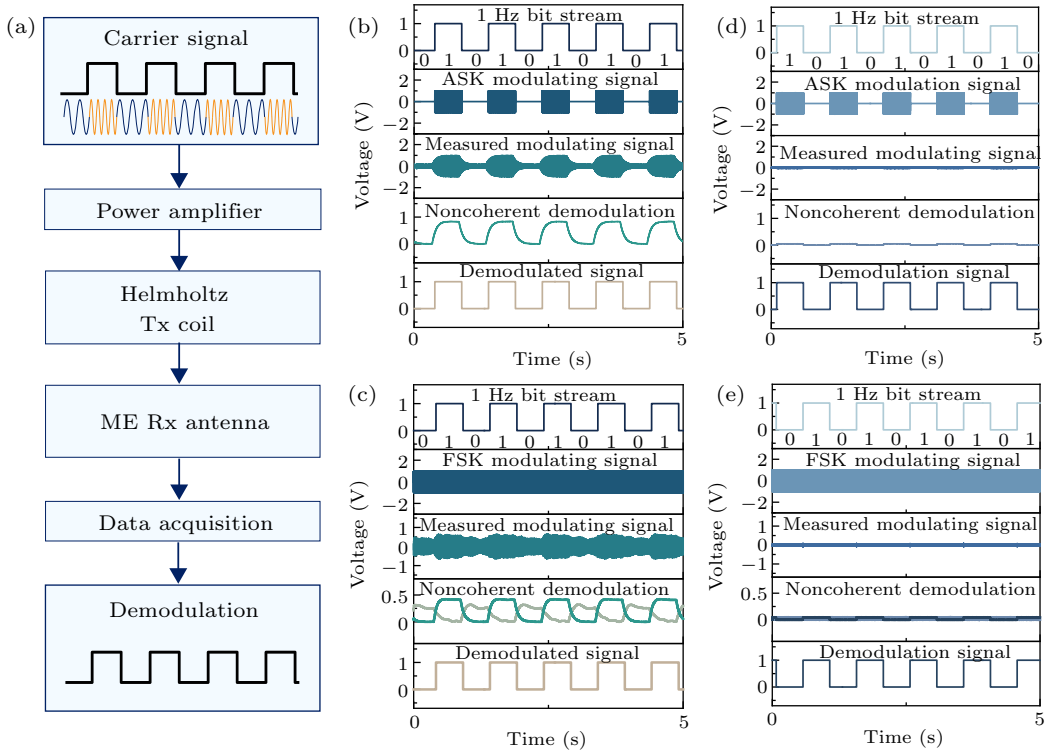


Fig. 6. (a) An experimental configuration diagram for testing the receiving capability of the ME antenna. Schematics of the 2ASK and 2FSK signal modulation and transmission of the bridge ME antenna (b)–(c) and classic ME antenna (d)–(e).

Table 1. Performance comparisons of different low-frequency ME receiving antennas.

Ref.	ME material	ME voltage coefficient (V/Oe)	NEB (fT/$\sqrt{\text{Hz}}$)	R_x area (cm^2)	Carrier frequency	Modulation mode
[26]	Metglas and PZT	3.8	260	9	23.95 kHz	DAM
[41]	Metglas and PZT	2.5	NA	0.0027	187 kHz	NA
[42]	Metglas and PVDF	0.55	NA	0.00175	49.9 kHz	NA
[43]	Terfenol-D and PZT	NA	NA	0.84	91.8 kHz	2ASK
[4]	Metglas and PMN-PT	70 nC/Oe	21.25	28	6.1 kHz and 18.4 kHz	2FSK
[44]	Metglas and PVDF	0.5	NA	17.5	44.9 kHz	2FSK
This work	Metglas and PMN-PT	104.1 nC/Oe	126	28	1089 Hz	2ASK and 2FSK (3 m)

5. Conclusion

The proposed ME antenna utilizes a bridge-supporting structure to excite three low-resonance frequencies (NEB $<$ 150 fT/$\sqrt{\text{Hz}}$) in the ULF band. This design yields a receiving antenna with low noise, high responsivity, and reliable signal reception capabilities for 2ASK/2FSK modulation. These distinctive capabilities demonstrate the potential of the proposed antenna for ULF communication technologies.

Data availability statement

The data that support the findings of this study are available from the corresponding author upon reasonable request.

Acknowledgements

This research was funded by the National Key Research and Development Program of China (Grant No. 2021YFA0716500) and the Shanghai Science and Technology Innovation Action Plan (Grant No. 21JC1402000).

References

[1] Tu C, Chu Z Q, Spetzler B, Hayes P, Dong C Z, Liang X F, Chen H H, He Y F, Wei Y Y, Lisenkov I, Lin H, Lin Y H, McCord J, Faupel F, Quandt E and Sun N X 2019 *Materials* **12** 2259
[2] Eerenstein W, Mathur N D and Scott J F 2006 *Nature* **442** 759
[3] Hassanien A E, Breen M, Li M H and Gong S B 2020 *Sci. Rep.* **10** 17006
[4] Zhang Q S, Xin B Y, Wu H Z, Hu L Z, Jiang T and Wang J 2023 *IEEE Antennas Wirel. Propag. Lett.* **23** 498

[5] Shen Y, Gao J Q, Hasanyan D, Wang Y J, Li M H, Li J F and Viehland D 2012 *Smart Mater. Struct.* **21** 115007

[6] Shen Y, McLaughlin K L, Gao J Q, Gray D, Hasanyan D and Wang Y J 2012 *IEEE Trans. Ultrason. Ferroelectr. Freq. Control.* **59** 2111

[7] Wu H Z, Tatarenko A, Bichurin M I and Wang Y J 2021 *Nano Energy* **83** 105777

[8] Gao J Q, Wang Z G, Shen Y, Li M H, Wang Y J, Finkel P, Li J F and Viehland D 2012 *Mater. Lett.* **82** 178

[9] Hu L Z, Wu H Z, You H R, Wang Y J and Gao A R 2021 *Sens. Actuators A Phys.* **332** 113100

[10] Burch H C, Garraud A, Mitchell M F, Moore R C and Arnold D P 2018 *IEEE Trans. Antennas Propag.* **66** 6265

[11] Bickford J A, McNabb R S, Ward P A, Freeman D K and Weinberg M S 2017 *Proceedings of the IEEE International Symposium on Antennas and Propagation & USNC/URSI National Radio Science Meeting*, July 9–14, 2017, San Diego, CA, USA, p. 1475

[12] Scott J F. Applications of modern ferroelectrics 2007 *Science* **315** 954

[13] Nan C W, Bichurin M I, Dong S X, Viehland D and Srinivasan G 2008 *J. Appl. Phys.* **103** 031101

[14] Shi Y, Li N and Yang Y 2021 *Chin. Phys. B* **30** 107503

[15] Zaeimbashi M, Lin H, Wang Z G, Chen H H, Emam S and Gao Y 2018 *Proceedings of the IEEE International Microwave Biomedical Conference (IMBioC)*, June 14–15, 2018, Philadelphia, PA, USA, p. 205

[16] Zaeimbashi M, Lin H, Wang Z G, Chen H H, Emam S and Gao Y 2019 *IEEE J. Electromagn. RF Microw. Med. Biol.* **3** 206

[17] Rangriz F, Khaleghi A and Balasingham I 2020 *Proceedings of the* 14*th European Conference on Antennas and Propagation (EuCAP)*, March 15–20, 2020, Copenhagen, Denmark, p. 1

[18] Yao Z, Wang Y E, Keller S and Carman G P 2015 *IEEE Trans. Antennas Propag.* **63** 3335

[19] Gao J Q, Shen Y, Finkel P, Blottman J, Li J F and Viehland D 2012 *Mater. Lett.* **88** 47

[20] Yang M T, Zhuang X, Sing M L C, Dolabdjian C, Goldstein D and Finkel P 2016 *IEEE Sens. J.* **16** 5557

[21] Shen L G, Li M H, Gao J Q, Shen Y, Li J F, Viehland D, Zhuang X, Sing M L C, Cordier C, Saez S and Dolabdjian C 2011 *J. Appl. Phys.* **110** 114510

[22] Jahns R, Greve H, Woltermann E, Quandt E and Knöchel R 2012 *Sens. Actuators A Phys.* **183** 16

[23] Zhai J Y, Dong S X, Xing Z P, Gao J Q, Li J F and Viehland D 2009 *J. Phys. D: Appl. Phys.* **42** 122001

[24] Park C S, Avirovik D, Bichurin M I, Petrov V M and Priya S 2012 *Appl. Phys. Lett.* **100** 212901

[25] Nan T X, Lin H, Gao Y, *et al.* 2017 *Nat. Commun.* **8** 296

[26] Dong C Z, He Y F, Li M H, Tu C, Chu Z Q, Liang X F, Chen H H, Wei Y Y, Zaeimbashi M and Wang X J 2020 *IEEE Antennas Wirel. Propag. Lett.* **19** 398

[27] Xu J R, Leung C M, Zhuang X, Li J F, Bhardwaj S, Volakis J and Viehland D 2019 *Sensors* **19** 853

[28] Gao J Q, Shen Y, Wang Y J, Finkel P, Li J F and Viehland D 2011 *IEEE Trans. Ultrason. Ferroelectr. Freq. Control.* **58** 1545

[29] Wang Y L, Zhang R, Sun E W, Song W and Cao W W 2013 *Chin. Phys. Lett.* **30** 096301

[30] Fang Z Q and Hou Z L 2018 *Chin. Phys. Lett.* **35** 054601

[31] Wu H Z, Jiang T, Liu Z, Fu S F, Cheng J W, You H R, Jiao J, Bichurin M, Sokolov O, Ivanov S and Wang Y J 2023 *Adv. Electron. Mater.* **9** 2300096

[32] Niu Y P and Ren H 2022 *IEEE Sens. J.* **22** 14008

[33] Zhai J Y, Xing Z P, Dong S X, Li J F and Viehland D 2006 *Appl. Phys. Lett.* **88** 062510

[34] Alsaleh R, Nasir A and Alshaikh I 2023 *Shock Vib.* **2023** 9524177

[35] Zhong Z Y, Zhang W M and Meng G 2013 *Sensors* **13** 15880

[36] Yu Y G, Li Y X, Zeng Y Q, Li J, Zuo L, Li Q and Zhang H W 2013 *Chin. Phys. B* **22** 077504

[37] Henthorn S, Ford K L and O'Farrell T 2019 *IEEE Trans. Antennas Propag.* **68** 111

[38] Schab K, Huang D Y and Adams J J 2019 *IEEE Access* **7** 30213

[39] Hu H Y, Zhang C, Li Y M and Jia W 2016 *Proceedings of the* 6*th International Conference on Electronics Information and Emergency Communication (ICEIEC)*, June 17–19, 2016, Beijing, China, p. 228

[40] Yue Y J, Liu L L and Yu R F 2014 *Proceedings of the International Conference on Software Intelligence Technologies and Applications & International Conference on Frontiers of Internet of Things*, December 4–6, 2014, Hsinchu, p. 212

[41] Kim W, Tuppen C A, Alrashdan F, Singer A, Weirnick R and Robinson J T 2023 *J. Appl. Phys.* **134** 094103

[42] Mukherjee D and Mallick D 2023 *Appl. Phys. Lett.* **122** 014102

[43] Lü X Z, Chen X, Zhang W Q, Gu L and Bao W M 2023 *IEEE Trans. Antennas Propag.* **71** 8493

[44] Mukherjee D and Mallick D A 2023 *Proceedings of the IEEE Microwaves, Antennas, and Propagation Conference (MAPCON)*, December 11–14, 2023, Ahmedabad, India, p. 1